AUT Journal of Electrical Engineering
10.22060/EEJ.2026.25436.5932

Electromagnetic Shielding Effectiveness of an Arbitrary-Shape Multilayered Anisotropic Composite Enclosure

Mona Kalantari[1]*, Seyed Hossein Hesamedin Sadeghi[1], Mitra Kalantari[2]
[1]Department of Electrical Engineering, Amirkabir University of Technology, Tehran, Iran
[2]Department of Computer Engineering, Islamic Azad University, Arak, Iran
[1*]Monakalantari92@aut.ac.ir ; [1]sadeghi@aut.ac.ir ; [2]mitrakalantari84@gmail.com

Abstract:

This paper uses an efficient surface integral equation-based MoM (SIE-MoM) scheme to study the electromagnetic shielding properties of arbitrary-shape multilayered anisotropic composite enclosures. In this scheme, each anisotropic composite layer is modeled by an equivalent homogeneous anisotropic medium with tensorial characteristics. The method treats each layer, separately, using the surface equivalence theorem. After applying the suitable boundary conditions, the SIEs solved by the Galerkin's-MoM. This computation includes, the expansion of equivalent surface current densities by proper basis functions, the rotation of dyadic Green's functions of the infinite space filled with the equivalent anisotropic material used for each layer, and finally the inner product of both sides of integral equations to express the SIEs in the form of matrix equations solved through an efficient inversion process of a sparse block-tridiagonal impedance matrix. The rotation angle of dyadic Green's functions is the angular deviation between the specified global coordinate system and the local principal one for anisotropic materials, which is determined by diagonalizing the permittivity tensor of the equivalent anisotropic layer defined in the global coordinate system. The validity and efficiency of the presented method are demonstrated for a three-layer irregular-shaped anisotropic composite enclosure by comparing the obtained results with those obtained using FE-solver of the commercial CST studio. Finally, a set of sensitivity analysis is done to examine the various parameters that affect the shielding properties of a two-layer cubic anisotropic composite enclosure.

Keywords: Composites, Anisotropic media, Surface integral equations, Method of moments, Shielding effectiveness.

1. Introduction

The increasing growth in the use of electrical and electronic packages requires the use of lightweight, sustainable, and tough materials for design and construction of supporting framework. Composites, as engineered synthetic materials, satisfy such multipurpose applications with their unique properties. In fact, common practical metals have limitations such as heavy weight, high production and maintenance cost, poor insulating properties, design inflexibility, and high susceptibility to chemical corrosion or physical damages against uneven environmental conditions [1-2]. These unfavorable properties can increase the risk of damages to the sensitive circuits embedded inside the chassis and force us to use of alternative composite materials which the mechanical and electrical properties are adjustable due to heterogeneous and layered nature. The composites having unique features of light weights, cheapness, longevity, good insulation properties (electrical and thermal), high mechanical stiffness, high corrosion and oxidation resistance, less creep, environmental stability, and design flexibility are more suitable options for chassis production. Despite all these properties, they exhibit lower effective equivalent electrical conductivity than metals, which is challenging in some electrical engineering applications, such as electromagnetic shielding, and useful in others, such as radome industries [3].

The electromagnetic shielding is an important topic in applied electromagnetics for mitigation of unwanted electromagnetic radiations emitted from high frequency electrical devices or ones coupled on sensitive electronic systems. Using suitable electromagnetic shielding enclosures around the main electronic components is one of the main solutions to control the passage of electromagnetic waves which can cause electromagnetic interferences (EMIs) [4].

A good EMI shielding against EMIs for a wideband frequency range is practically obtained using conductive and ferromagnetic materials which are used for mitigation of electric and magnetic fields, respectively. Composites are made by two main separate phases named, reinforcing fillers (made of carbon, copper, gold, silver, glass, and etc.) incorporated in a matrix substrate (made of epoxy resin, polyester, polymer, Teflon, and etc.). Therefore, the provided effective equivalent electromagnetic characteristics are adjustable for various applications and dependent on the electromagnetic properties

and fractional volume of both phases. For example, conductive carbon fiber reinforced composites (CFRC) have been introduced as a suitable alternative to metals for providing a high value of shielding effectiveness (SE) [5-7]. In a different application, glass fiber reinforced plastic composites (GFRPC) with low SE and maximum transmission are used for manufacturing radomes which protect antennas against mechanical damages [8].

In addition. composites are usually made in multiple layers. The multilayered nature of composites provides more degrees of freedom to control the wave propagation. Depending on the thickness and concentration of conductive inclusions or fibers in each layer, it can transmit, reflect, and absorb the power of electromagnetic waves which are the three main mechanisms for shielding [9-10]. Therefore, the optimal shielding for a composite enclosure can be achieved by stacking different layers of composite materials in barrier walls. In cases, the conductive reinforcing fibers are embedded inside the matrix in parallel to each other, the composite layer can be treated as an effective equivalent anisotropic homogeneous media which inherently presents more flexibility due to the expression of electromagnetic characteristics in tensorial form [11-12].

Different methods have been proposed to study the electromagnetic behavior of multilayer anisotropic structures. For example, analytical methods have been used for planar [13], cylindrical [14], and spherical [15] geometries. These methods are simple and accurate for canonical geometries; but they become hard to use for complex structures. In contrast, the numerical methods that have been widely used with the development of computational capabilities, can treat complicated structures and provide sufficient accuracy using a full-wave solution of Maxwell's equations [16]. Basic types of these methods that have been implemented to analyze multilayer anisotropic composite structures are named, finite difference time domain (FDTD) [17], finite element (FE) [12], [18], and method of moments (MoM) [7]. FDTD and FE are very common methods for computational solving of time dependent and steady-state electromagnetic problems, respectively. These numerical solutions are based on fine enough volumetric discretization of the entire spaces existing in the problem and limited by applying the absorbing boundary conditions to stop the calculations. Accordingly, the need for the processor execution time and computational memory increases unfavorably. Especially, these

methods will miss the proper accuracy and efficiency in the design and microscopic analysis of large-scale multilayer anisotropic composite structures at high frequencies. In contrast, The MoM is a frequency-domain integral-equation based method without requiring to discretize a large volume of space around a given geometry of interest. In fact, in the MoM, only the sources are discretized for the unknown equivalent electric and magnetic current densities. Therefore, the computational costs will inevitably decrease compared to the previous methods [19]. Dealing with all the layers and boundaries of an arbitrary shape multilayer composite structure with tensorial representation of the equivalent electromagnetic characteristics of each layer will lead to the formation of volume integral equations (VIEs), whose solution by MoM (VIE-MoM) will perform by inversion of an excessively large impedance matrix, requiring very high or even unavailable computational resources [20]. This issue leads the problem to be more challenging or unsolvable when the dimensions, frequency, or number of different anisotropic composite layers with tensorial properties increases. In addition, the VIE-MoM scheme requires the complex mathematical calculations of the dyadic Green's functions for any arbitrary shape multilayer anisotropic composite object which will be unusable even for another similar structure. For example, the general form of 3-D static Green's function for a general structure consisting of *N*-arbitrary adjacent dielectric wedges is derived using the Kontorovich–Lebedev and Fourier transforms in [21], where used in the case of a vertically stratified two-layer half-space. These drawbacks limit the use of VIE-MoM and then, the use of SIEs in conjunction with MoM (SIE-MoM) has been proposed [22]. In this approach, the surface equivalence theorem is used and only the interfaces between the consecutive or adjacent layers of a heterogeneous composite object are discretized to obtain the unknown equivalent electric and magnetic surface current densities. Therefore, the size of the impedance matrix is much smaller than VIE-MoM scheme and the inversion process will have lower computational time and memory. Also, the required dyadic Green's functions of various anisotropic layers are corresponding to the case of infinite space that filled with the relevant anisotropic material. In general, this is the more superiority of the SIE-MoM compared to the VIE-MoM, where the dyadic Green's functions must be calculated separately for any multilayer anisotropic composite object of interest.

Modeling multilayered composite-based structures in microscopic scale is impossible for numerical studies due to the heterogeneous nature of composite layers. Therefore, it is necessary to use homogenization techniques of anisotropic composite layers and represent the electromagnetic properties of each layer by an equivalent tensor of permittivity, permeability or conductivity [18]. Once, the homogenization technique is used, each layer can be defined as a standard anisotropic homogeneous layer and the problem is reduced to solving a multilayer anisotropic object with the SIE-MoM scheme [23].

Another way to more reduce the complexity of problem solution is the optimization of the conventional SIE-MoM scheme, where the simultaneous dealing with all interfaces between consecutive anisotropic layers with tensorial properties, causes an undesirable increase in the number of unknown surface current densities and subsequently, the number of the impedance matrix elements by 9-times compared to solving the problem of a composite target containing various isotropic layers whose properties are represented by a complex scalar number. Therefore, the inversion process requires a lot of computing time and memory to treat all surfaces simultaneously and reverse at once. In addition, the common approach can cause more numerical issues such as ill-conditioning of the impedance matrix and growth of errors in the calculation of its elements.

To overcome mentioned computational issues, we have recently presented a novel study, where an efficient SIE-MoM was extended for computing the shielding effectiveness of a multilayer composite enclosure with arbitrary geometry [7]. In this scheme, each composite layer including fibers oriented in random directions is treated separately and modeled by an effective equivalent homogeneous isotropic lossy medium. The MoM implementation leads to the formation of a block-tridiagonal impedance matrix with scalar elements. Using efficient block-by-block inversion process, the computational costs have been improved significantly compared to the traditional matrix inversion techniques. However, this method remains applicable only for equivalent isotropic layers.

In another recent study, we have expanded the new SIE-MoM scheme proposed in [7] for analysis the electromagnetic scattering from an arbitrary-shape multilayer anisotropic object, where the dyadic Green’s functions are not readily available [23]. In this study, we utilize the dyadic Green’s functions

of infinite anisotropic space, rotated by the angle of deviation between the adopted global coordinate system and the local principal coordinate system of each anisotropic layer. This angle is determined by diagonalizing the full dielectric tensor of the anisotropic layer of interest given in the global coordinate system. Using standard Galerkin's-MoM solution of the so-obtained SIEs, the resulting impedance matrix takes a sparse block-tridiagonal form where, each block has small size and condition number leading to manageable computation. Next, using the blocks including tensorial elements in an efficient block-by-block inversion process, enhances the computational efficiency compared to other similar methods.

This paper aims to use the new efficient SIE-MoM scheme presented in [23] for analyzing the electromagnetic shielding effectiveness of an arbitrary-shape multilayer anisotropic composite enclosure. According to our knowledge, it's the first time that an accurate and fast SIE-MoM approach is implemented for this purpose. After modeling each composite layer as an effective equivalent anisotropic homogeneous media, rotating the global coordinate system by diagonalizing of permittivity tensors, the electromagnetic fields are treated in each layer, separately. Then, using an efficient block-by-block inversion process significantly improves the computational burden. Finally, a set of sensitivity analysis is performed where the effects of the diameter of reinforcing fibers, thickness of layers, real and imaginary (electrical conductivity) parts of the dielectric constant of both matrix and reinforcing phases of various layers, and polarization of incident plane wave on the shielding effectiveness of the two-layer rectangular enclosure are studied.

The organization of this paper is as follows. The geometry of the problem and homogenization of the composite layers, boundary conditions and a summary of the matrix equations are expressed in section. 2. The validity and efficiency of the method for a three-layer arbitrary geometry anisotropic composite enclosure and study the effects of various parameters on the shielding effectiveness of a two-layer cubic enclosure are performed in section. 3. Finally, the conclusions of this paper are given in section. 4.

2. Formulation

2-1- Geometry and Modeling

10.22060/EEJ.2026.25436.5932

The geometry of the problem is shown in Fig. 1 where the electromagnetic fields of a plane wave illuminate an arbitrary-shape multilayer anisotropic composite enclosure with the time-harmonic of $e^{-j\omega t}$, where $\omega = 2\pi f$ is the angular frequency of operation. It is assumed that the composite object is non-magnetic and the tensorial permittivity constant of the lth ($l = 1, 2, \ldots, L$) anisotropic composite layer is considered as $\overline{\overline{\varepsilon}}_l = \varepsilon_0 \overline{\overline{\varepsilon}}_{r,l}$, where ε_0 is the permittivity of free space. First, we follow the procedure described in [23], where the dyadic Green's functions of free space filled with the respective anisotropic composite layer having parallel cylindrical reinforcing fibers are rotated by the deviation angle between the global *xyz* coordinate system (Fig. 1) and the respective local principal coordinate system in the lth layer ($x_l' y_l' z_l'$). Aligning the global *xyz* system with the local principal system of each layer is equivalent to diagonalization of the full permittivity tensor of the composite layer of interest which can be done as follows,

$$\overline{\overline{\varepsilon}}'_{r,l} = [\overline{\overline{P}}_l]^{-1} \overline{\overline{\varepsilon}}_{r,l} [\overline{\overline{P}}_l] \tag{1}$$

where $[\overline{\overline{P}}_l]$ is the orthogonal matrix, including $\overline{\overline{\varepsilon}}_{r,l}$ eigenvectors in the global coordinate system (Fig. 1). Then, we can represent the diagonalized form of the permittivity, $\overline{\overline{\varepsilon}}'_{r,l}$, as follows,

$$\overline{\overline{\varepsilon}}'_{r,l} = \varepsilon'_{\perp,l} \overline{\overline{I}} + (\varepsilon'_{\parallel,l} - \varepsilon'_{\perp,l}) \hat{c}_l^T . \hat{c}_l \tag{2}$$

where, $\hat{c}_l$ is the unit vector of the parallel reinforcing fibers orientation in the lth layer which named as the principal axis. Also, $\varepsilon'_{\parallel,l}$ and $\varepsilon'_{\perp,l}$ are, respectively, the relative permittivity along the directions parallel and perpendicular to $\hat{c}_l$ (cylindrical fiber axis), and $\overline{\overline{I}}$ represents the identity dyad.

10.22060/EEJ.2026.25436.5932

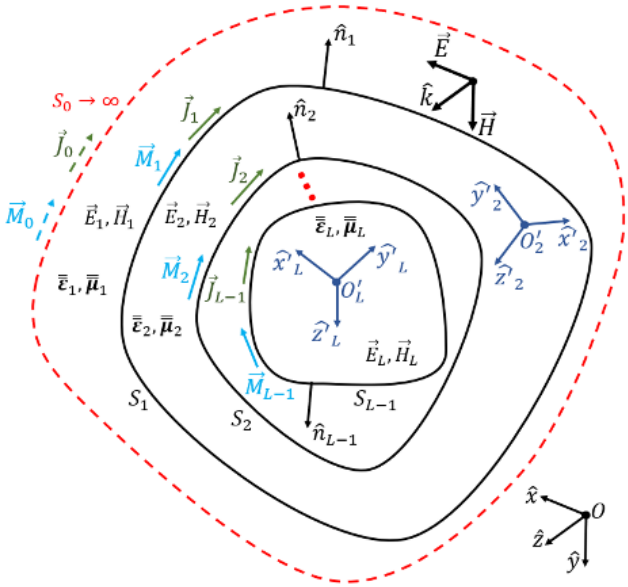

Fig. 1. Cross-section view of an arbitrary shape *L*-layer anisotropic structure, with the global coordinates (*xyz*) and local principal coordinates ($x_l^{'} y_l^{'} z_l^{'}$) in the *l*-th layer (*l* =1: *L*) [23].

Now, by using the homogenization technique for single-layer modeling of each composite layer [12] which have good accuracy for microscopic composite dimensions much smaller than the wavelength, the elements of the matrix represented in (2) are obtained as,

$$\varepsilon_{\|,l}^{-1} = (1-v_l)\varepsilon_{\mathrm{m},l}^{-1} + v_l \varepsilon_{\mathrm{f},l}^{-1} \tag{3a}$$

$$\varepsilon_{\perp,l} = (1-v_l)\varepsilon_{\mathrm{m},l} + v_l \varepsilon_{\mathrm{f},l} \tag{3b}$$

where, the permittivity of the parallel reinforcing fibers, $\varepsilon_{\mathrm{f},l}$, the permittivity of the matrix phase, $\varepsilon_{\mathrm{m},l}$, and the volume fraction of reinforcing fibers, *v*, in the *l*th ($l = 1, 2, \ldots, L$) composite layer obtained as follows,

$$\varepsilon_{\mathrm{m},l} = \varepsilon_0 \left(\varepsilon_{\mathrm{r_m},l} + j \frac{\sigma_{\mathrm{m},l}}{\varepsilon_0 \omega} \right) \tag{4a}$$

$$\varepsilon_{\mathrm{f},l} = \varepsilon_0 \left(\varepsilon_{\mathrm{r_f},l} + j \frac{\sigma_{\mathrm{f},l}}{\varepsilon_0 \omega} \right) \tag{4b}$$

$$v_l = \frac{\pi d_l^{\,2}}{4 s_l w_l} \tag{4c}$$

where, $\varepsilon_{\mathrm{r_m},l}$ and $\sigma_{\mathrm{m},l}$ are, respectively, the relative permittivity and the electrical conductivity constants of the matrix, respectively. Also, $\varepsilon_{\mathrm{r_f},l}$ is the relative permittivity of the parallel conductive fibers in the *l*th ($l = 1, 2, \ldots, L$) layer. Referring to Fig. 2, d_l and s_l denote the diameter and center-to-center distance of adjacent embedded fibers in the *l*th layer with the thickness of w_l [12].

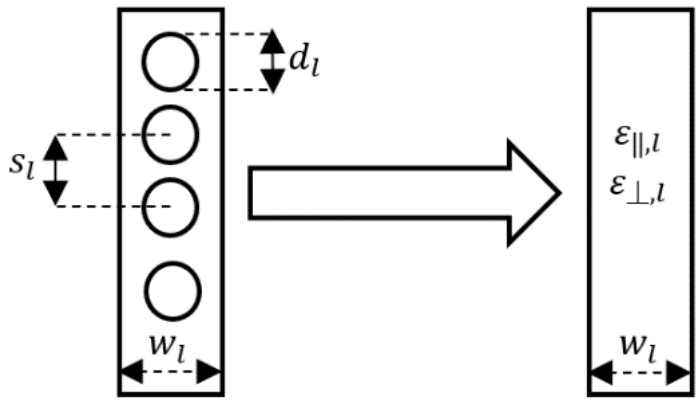

Fig. 2. Modeling the *l*th ($l = 1, 2, \ldots, L$) composite layer having parallel conductive reinforcing fibers with effective equivalent anisotropic homogeneous media.

2-2- Scattered Fields and Boundary Conditions

According to the surface equivalence theorem, the scattered electric and magnetic fields in the *l*th ($l = 1,2,\ldots,L$) layer of the structure shown in Fig. 1 are caused by the equivalent electric and magnetic surrounding surface current densities on the *l*th ($\vec{J}_l$ and $\vec{M}_l$) and the (*l*-1)th ($\vec{J}_{l-1}$ and $\vec{M}_{l-1}$) consecutive interfaces, *i.e.*,

$$\vec{X}_{\mathrm{sc},l} = \vec{X}_{\mathrm{sc},l}\left(\vec{J}_l, \vec{M}_l\right) + \vec{X}_{\mathrm{sc},l}\left(-\vec{J}_{l-1}, -\vec{M}_{l-1}\right) \;\; ; \;\; \vec{X} \in \left\{\vec{E}, \vec{H}\right\} \tag{5}$$

After aligning the global *xyz* coordinate system with the local principal system of the *l*th equivalent anisotropic layer ($x_l' y_l' z_l'$), we use of the rotated local dyadic Green's functions of the infinite space filled with the respective anisotropic material to determine the integrals of the scattered electric and magnetic fields as follows,

$$\vec{E}_{\mathrm{sc},l}\left(\vec{J}_l,\vec{M}_l\right)=\int_{S_l}\left([\bar{\bar{\mathrm{P}}}_l]\,\bar{\bar{G}}_{\mathrm{ee},l}(\vec{r},\vec{r}')\,[\bar{\bar{\mathrm{P}}}_l]^{-1}\right).\vec{J}_l(\vec{r}')d\vec{r}'+\int_{S_l}\left([\bar{\bar{\mathrm{P}}}_l]\,\bar{\bar{G}}_{\mathrm{em},l}(\vec{r},\vec{r}')\,[\bar{\bar{\mathrm{P}}}_l]^{-1}\right).\vec{M}_l(\vec{r}')d\vec{r}' \tag{6a}$$

$$\vec{H}_{\mathrm{sc},l}\left(\vec{J}_l,\vec{M}_l\right)=\int_{S_l}\left([\bar{\bar{\mathrm{P}}}_l]\,\bar{\bar{G}}_{\mathrm{me},l}(\vec{r},\vec{r}')\,[\bar{\bar{\mathrm{P}}}_l]^{-1}\right).\vec{J}_l(\vec{r}')d\vec{r}'+\int_{S_l}\left([\bar{\bar{\mathrm{P}}}_l]\,\bar{\bar{G}}_{\mathrm{mm},l}(\vec{r},\vec{r}')\,[\bar{\bar{\mathrm{P}}}_l]^{-1}\right).\vec{M}_l(\vec{r}')d\vec{r}' \tag{6b}$$

where $\bar{\bar{G}}_{\mathrm{ee},l}$, $\bar{\bar{G}}_{\mathrm{em},l}$, $\bar{\bar{G}}_{\mathrm{me},l}$ and $\bar{\bar{G}}_{\mathrm{mm},l}$ are named, respectively, the electric-electric, electric-magnetic, magnetic-electric, and magnetic-magnetic dyadic Green's functions. After calculating the total electromagnetic fields in the *l*th layer by summation of the incident fields *i.e.*, $\vec{E}_{\mathrm{in},l}$ and $\vec{H}_{\mathrm{in},l}$ (if exist) and those obtained using (6a) and (6b), we can apply the appropriate boundary conditions on each interface $S_l\,(l=0,1,\ldots.,L-1)$, separating the *l*th and (*l*+1)th layers with the outward unit normal vector of n_l (Fig. 1) as follows [23],

$$\begin{aligned}&n_l\times n_l\times\left[[\bar{\bar{\mathrm{P}}}_l].\,\vec{E}_{\mathrm{in},l}(\vec{r})-[\bar{\bar{\mathrm{P}}}_l].\,\vec{E}_{\mathrm{in},l+1}(\vec{r})\right]_{|\vec{r}\to S_l}=n_l\times n_l\times\\&\Bigg[-\int_{S_l}\left([\bar{\bar{\mathrm{P}}}_l]\,\bar{\bar{G}}_{\mathrm{ee},l}(\vec{r},\vec{r}')\,[\bar{\bar{\mathrm{P}}}_l]^{-1}\right).\vec{J}_l(\vec{r}')d\vec{r}'-\int_{S_l}\left([\bar{\bar{\mathrm{P}}}_l]\,\bar{\bar{G}}_{\mathrm{em},l}(\vec{r},\vec{r}')\,[\bar{\bar{\mathrm{P}}}_l]^{-1}\right).\vec{M}_l(\vec{r}')d\vec{r}'\\&+\int_{S_{l-1}}\left([\bar{\bar{\mathrm{P}}}_l]\,\bar{\bar{G}}_{\mathrm{ee},l}(\vec{r},\vec{r}')\,[\bar{\bar{\mathrm{P}}}_l]^{-1}\right).\vec{J}_{l-1}(\vec{r}')d\vec{r}'+\int_{S_{l-1}}\left([\bar{\bar{\mathrm{P}}}_l]\,\bar{\bar{G}}_{\mathrm{em},l}(\vec{r},\vec{r}')\,[\bar{\bar{\mathrm{P}}}_l]^{-1}\right).\vec{M}_{l-1}(\vec{r}')d\vec{r}'\\&+\int_{S_{l+1}}\left([\bar{\bar{\mathrm{P}}}_l]\,\bar{\bar{G}}_{\mathrm{ee},l+1}(\vec{r},\vec{r}')\,[\bar{\bar{\mathrm{P}}}_l]^{-1}\right).\vec{J}_{l+1}(\vec{r}')d\vec{r}'+\int_{S_{l+1}}\left([\bar{\bar{\mathrm{P}}}_l]\,\bar{\bar{G}}_{\mathrm{em},l+1}(\vec{r},\vec{r}')\,[\bar{\bar{\mathrm{P}}}_l]^{-1}\right).\vec{M}_{l+1}(\vec{r}')d\vec{r}'\\&-\int_{S_l}\left([\bar{\bar{\mathrm{P}}}_l]\,\bar{\bar{G}}_{\mathrm{ee},l+1}(\vec{r},\vec{r}')\,[\bar{\bar{\mathrm{P}}}_l]^{-1}\right).\vec{J}_l(\vec{r}')d\vec{r}'-\int_{S_l}\left([\bar{\bar{\mathrm{P}}}_l]\,\bar{\bar{G}}_{\mathrm{em},l+1}(\vec{r},\vec{r}')\,[\bar{\bar{\mathrm{P}}}_l]^{-1}\right).\vec{M}_l(\vec{r}')d\vec{r}'\Bigg]_{|\vec{r}\to S_l}\end{aligned} \tag{7a}$$

$$
\begin{aligned}
& n_l \times n_l \times \left[[\bar{\bar{\mathrm{P}}}_l].\, \vec{H}_{\mathrm{in},l}(\vec{r}) - [\bar{\bar{\mathrm{P}}}_l].\, \vec{H}_{\mathrm{in},l+1}(\vec{r}) \right]_{\vec{r}\to S_l} = n_l \times n_l \times \\
& \Bigg[-\int_{S_l} \left([\bar{\bar{\mathrm{P}}}_l]\, \bar{\bar{G}}_{\mathrm{me},l}\, [\bar{\bar{\mathrm{P}}}_l]^{-1} \right).\vec{J}_l(\vec{r}')d\vec{r}' - \int_{S_l} \left([\bar{\bar{\mathrm{P}}}_l]\, \bar{\bar{G}}_{\mathrm{mm},l}\, [\bar{\bar{\mathrm{P}}}_l]^{-1} \right).\vec{M}_l(\vec{r}')d\vec{r}' \\
& + \int_{S_{l-1}} \left([\bar{\bar{\mathrm{P}}}_l]\, \bar{\bar{G}}_{\mathrm{me},l}\, [\bar{\bar{\mathrm{P}}}_l]^{-1} \right).\vec{J}_{l-1}(\vec{r}')d\vec{r}' + \int_{S_{l-1}} \left([\bar{\bar{\mathrm{P}}}_l]\, \bar{\bar{G}}_{\mathrm{mm},l}\, [\bar{\bar{\mathrm{P}}}_l]^{-1} \right).\vec{M}_{l-1}(\vec{r}')d\vec{r}' \\
& + \int_{S_{l+1}} \left([\bar{\bar{\mathrm{P}}}_l]\, \bar{\bar{G}}_{\mathrm{me},l+1}\, [\bar{\bar{\mathrm{P}}}_l]^{-1} \right).\vec{J}_{l+1}(\vec{r}')d\vec{r}' + \int_{S_{l+1}} \left([\bar{\bar{\mathrm{P}}}_l]\, \bar{\bar{G}}_{\mathrm{mm},l+1}\, [\bar{\bar{\mathrm{P}}}_l]^{-1} \right).\vec{M}_{l+1}(\vec{r}')d\vec{r}' \\
& - \int_{S_l} \left([\bar{\bar{\mathrm{P}}}_l]\, \bar{\bar{G}}_{\mathrm{me},l+1}\, [\bar{\bar{\mathrm{P}}}_l]^{-1} \right).\vec{J}_l(\vec{r}')d\vec{r}' - \int_{S_l} \left([\bar{\bar{\mathrm{P}}}_l]\, \bar{\bar{G}}_{\mathrm{mm},l+1}\, [\bar{\bar{\mathrm{P}}}_l]^{-1} \right).\vec{M}_l(\vec{r}')d\vec{r}' \Bigg]_{\vec{r}\to S_l}
\end{aligned}
\tag{7b}
$$

2-3- MoM Implementation and Shielding Effectiveness Computation

To solve the integral equations in (7a) and (7b), we use of Galerkin's-MoM [16]. At first, we use of the RWG basis functions for expanding the unknown equivalent electric ($\vec{J}_l$) and magnetic ($\vec{M}_l$) surface current densities on $S_l\,(l = 0, 1, \ldots, L-1)$. Next, we use the inner product of the RWG weight functions to both sides of (7a) and (7b) to obtain respective matrix equation as $[\bar{\bar{\mathrm{Z}}}][\mathbf{I}] = [\mathbf{V}]$. The details of this process for uniaxial anisotropic layers described in [23]. In this way, the impedance matrix takes a sparse tridiagonal block form as (8) with well-conditioned dyadic blocks. First, according to (9a), the inverse of main diagonal blocks are calculated and then, they are used for calculating the inverse of side blocks in a fast recursive mathematical manipulation, (see. 9b). After, applying efficient block-by-block inversion process, the unknown equivalent current densities will be calculated as $[\mathbf{I}] = [\bar{\bar{\mathrm{Z}}}]^{-1}[\mathbf{V}]$.

$$
[\bar{\bar{Z}}] = \begin{bmatrix}
\bar{\bar{[\mathrm{z}]}}_{0,0} & \bar{\bar{[\mathrm{z}]}}_{0,1} & 0 & \cdots & 0 \\
\bar{\bar{[\mathrm{z}]}}_{1,0} & \bar{\bar{[\mathrm{z}]}}_{1,1} & \bar{\bar{[\mathrm{z}]}}_{1,2} & \cdots & 0 \\
0 & \bar{\bar{[\mathrm{z}]}}_{2,1} & \bar{\bar{[\mathrm{z}]}}_{2,2} & \ddots & \vdots \\
\vdots & \vdots & \ddots & \ddots & \bar{\bar{[\mathrm{z}]}}_{L-2,L-1} \\
0 & 0 & \cdots & \bar{\bar{[\mathrm{z}]}}_{L-1,L-2} & \bar{\bar{[\mathrm{z}]}}_{L-1,L-1}
\end{bmatrix}
\tag{8}
$$

$$\overline{\overline{[z]}}^{-1}_{l,l} = [\overline{\overline{[z]}}_{l,l} - \overline{\overline{[X]}}_{l} - \overline{\overline{[Y]}}_{l}]^{-1} \quad ; \quad (l = l') \tag{9a}$$

$$\overline{\overline{[z]}}^{-1}_{l,l'} = \begin{cases} -[\overline{\overline{[z]}}_{l,l} - \overline{\overline{[X]}}_{l}]^{-1} \left(\overline{\overline{[z]}}_{l,l-1}\right)\left(\overline{\overline{[z]}}^{-1}_{l-1,l'}\right) & ; \quad l \rangle l' \\ -[\overline{\overline{[z]}}_{l,l} - \overline{\overline{[Y]}}_{l}]^{-1} \left(\overline{\overline{[z]}}_{l,l+1}\right)\left(\overline{\overline{[z]}}^{-1}_{l+1,l'}\right) & ; \quad l \langle l' \end{cases} \tag{9b}$$

where

$$\overline{\overline{X}}_{l-1} = \begin{cases} 0 & ; \quad l = L \\ \overline{\overline{z}}_{l-1,l}[\overline{\overline{z}}_{l,l} - \overline{\overline{X}}_{l}]^{-1}\overline{\overline{z}}_{l,l-1} & ; \quad 0 \langle l \leq L-1 \end{cases} \tag{9c}$$

$$\overline{\overline{Y}}_{l+1} = \begin{cases} 0 & ; \quad l = -1 \\ \overline{\overline{z}}_{l+1,l}[\overline{\overline{z}}_{l,l} - \overline{\overline{Y}}_{l}]^{-1}\overline{\overline{z}}_{l,l+1} & ; \quad 0 \leq l \langle L-1 \end{cases} \tag{9d}$$

Once we calculate the equivalent surface current densities, the obtained total electric and magnetic fields inside the enclosure, ($\vec{E}_L$ and $\vec{H}_L$), can be used to calculate the *i*th component of the electric shielding effectiveness of the enclosure, SE_i^E, and magnetic one, SE_i^H, as follows,

$$\mathrm{SE}_i^E\,(\mathrm{dB}) = -20\log\left(\frac{|\vec{E}_L^{\,i}|}{|\vec{E}_{\mathrm{in},1}|}\right) \quad , \quad i = x, y, z \tag{10a}$$

$$\mathrm{SE}_i^H\,(\mathrm{dB}) = -20\log\left(\frac{|\vec{H}_L^{\,i}|}{|\vec{H}_{\mathrm{in},1}|}\right) \quad , \quad i = x, y, z \tag{10b}$$

3. Numerical Results and Discussion

The expanded method has been used to examine the computational efficiency for the results of shielding effectiveness of a three-layer irregular-shape anisotropic composite enclosure compared to those obtained using the FE solver of the well-known Computer Simulation Technology (CST) studio [24]. Also, a set of sensitivity analysis is done where the effects of the diameter of the reinforcing fibers, the thickness of various layers, the relative permittivity of the matrix phase of layers, the electrical conductivity of the fibers, and the polarization of the incident plane wave on a two-layer

10.22060/EEJ.2026.25436.5932

cubic anisotropic composite enclosure are studied. All results are obtained by an Intel Core i7 @ 4.2 GHz processor, with 64 GB of RAM. Also, for making a uniform mesh in all studies, the value of the cell size with respect to the wavelength is considered 14.

3-1-Three-Layer Irregular-Shape Anisotropic Composite Enclosure

To show the generality of the expanded method for arbitrary geometry, we focus on a three-layer irregular-shape anisotropic composite enclosure illuminated by a x-polarized plane wave, propagating in the $\hat{z}$-direction in free space.

Referring to Fig. 3, the dimensions of the structure are as follows, a =120 mm, b =100 mm, c = 80 mm, and d = 50 mm, D_1 = 100 mm, D_2 = 80 mm, D_3 = 60 mm, and D_4 = 30 mm [23]. The host materials in the first and second composite layers with the thickness of $w_{1,2}$= 20 mm is considered epoxy resin ($\varepsilon_{r,e}$ = 3.4), having the $\hat{z}$-oriented cylindrical carbon fibers with $\varepsilon_{r,f}$ = 4 (σ_{f_1} = 10000 S/m, d_{f_1} = 1 mm, s_1= 12 mm (see. Fig. 2) in the former and the oriented carbon fibers parallel to y-axis (σ_{f_2} = 10000 S/m, d_{f_2} = 1.5 mm, s_2= 10 mm) in the latter. Finally, the host material in the third layer (w_3= 30 mm) is considered Teflon ($\varepsilon_{r,t}$ = 2.2) with the x-oriented fibers (σ_{f_3} = 70000 S/m, d_{f_3} = 3 mm, s_3= 5 mm). Accordingly, the fiber volume fraction in three layers is, respectively, v_1= 0.33%, v_2= 0.88%, and v_3= 4.71% where, the inner layer is considered more lossy to avoid internal resonance effects.

The frequency dependence of the equivalent parallel and perpendicular relative permittivity of various anisotropic composite layers are shown in Figs. (4a)-(4c). As can be seen from these figures, the imaginary part of the perpendicular permittivity is much more than parallel part, which made very large loss and SE in the direction perpendicular to the axis of the reinforcing fibers.

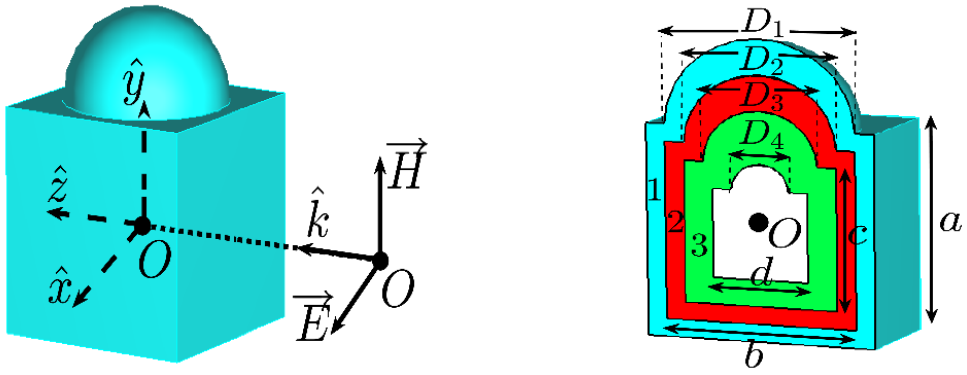

(a) (b)

Fig. 3. (a) 3D and (b) 2D views of a three-layer irregular-shape anisotropic composite enclosure.

Variations of the *x*-component of the SE_x^E and *y*-component of the magnetic shielding effectiveness (SE_y^H) for various frequencies at the center of the cubic part of the enclosure are plotted in Fig. 5. For comparison purpose, the results are compared with those obtained using the FE-solver of well-known Computer Simulation Technology (CST) studio. A study of the results in Fig. 5 illustrates a good agreement between the two set of results, substantiating the accuracy of the proposed method for analyzing anisotropic composite structures. It should be noted that more details on the accuracy and convergence of the method have been studied in [23].

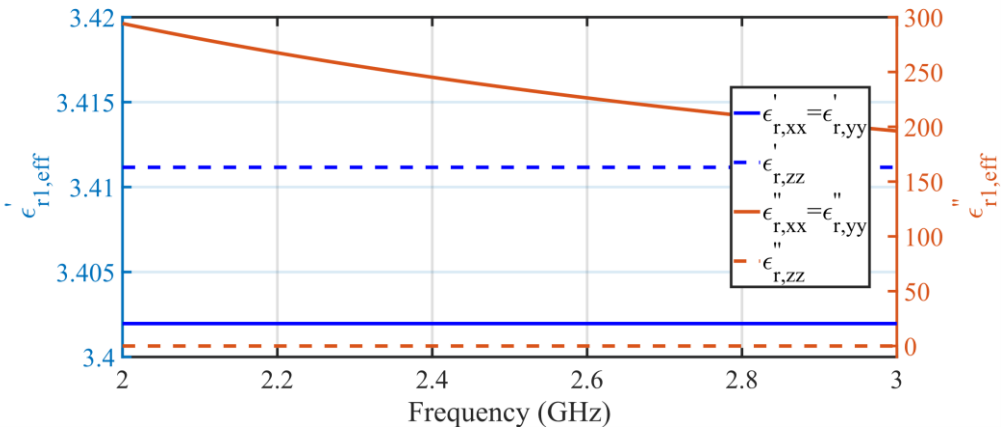

(a)

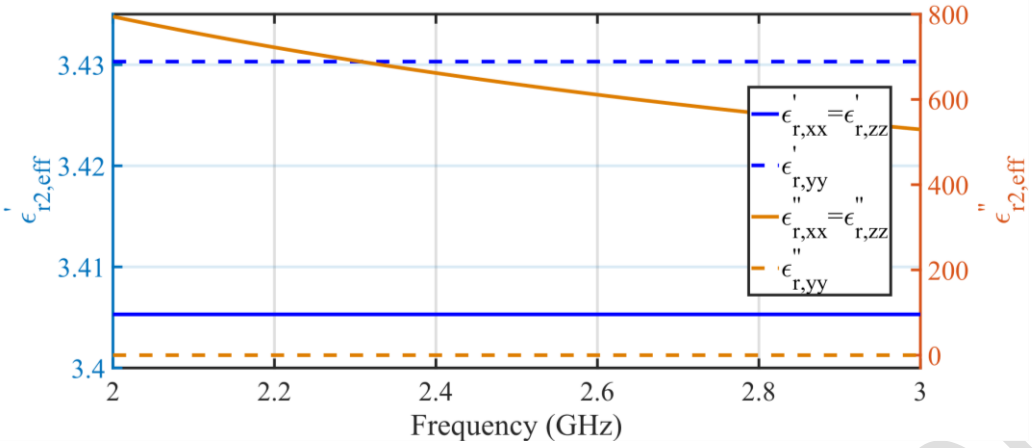

(b)

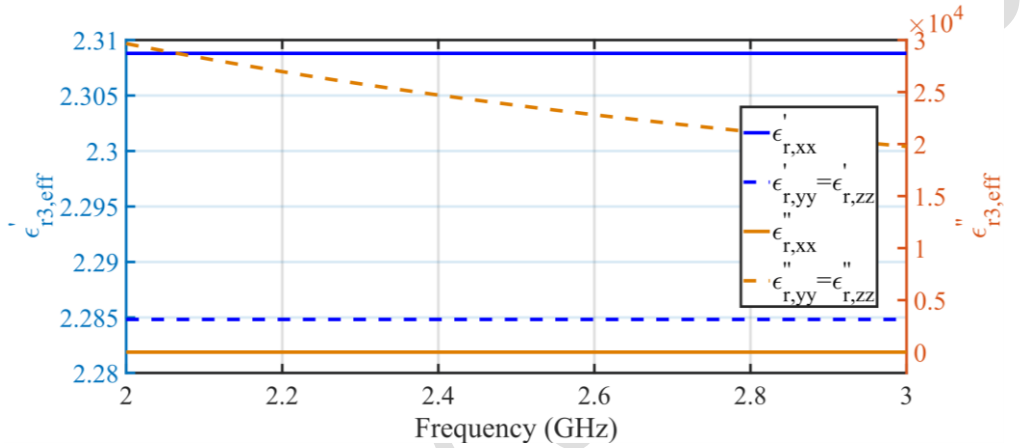

(c)

Fig. 4. Frequency dependence of real ($\varepsilon'_{r,eff}$) and imaginary ($\varepsilon''_{r,eff}$) parts of the equivalent parallel and perpendicular relative permittivity of the a) the first, b) the second, and c) the third anisotropic composite layers of the structure shown in Fig. 3.

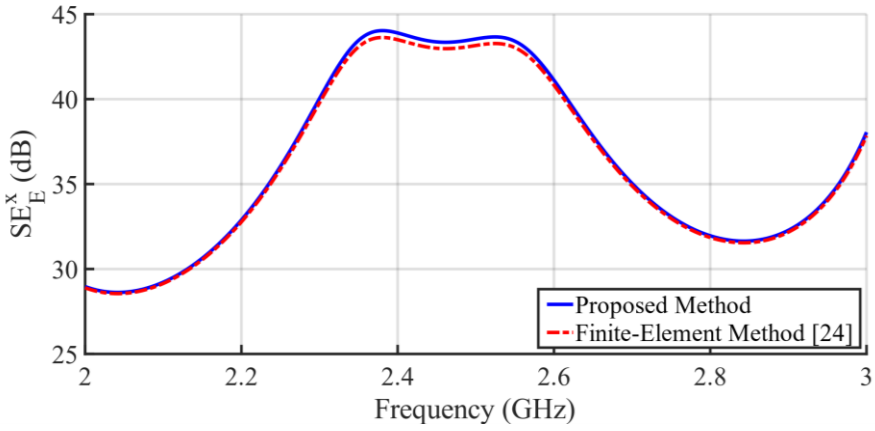

(a)

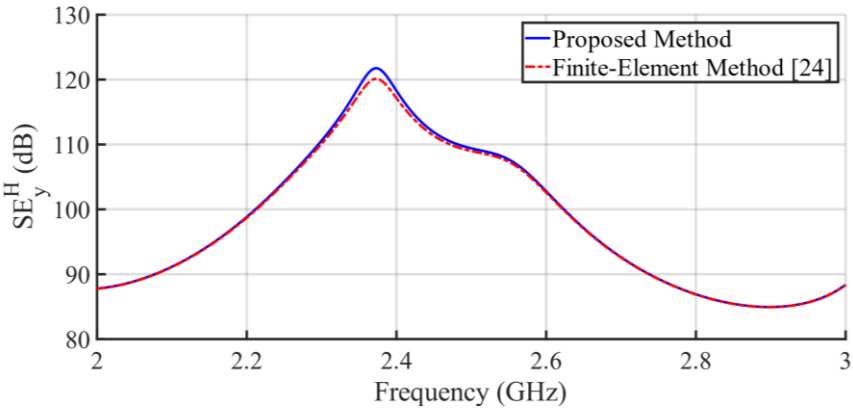

(b)

Fig. 5. Variations of the a) *x*-component of the electric shielding effectiveness (SE_x^E) and b) *y*-component of the magnetic shielding effectiveness (SE_y^H) at the center of the cubic part of the enclosure shown in Fig. 3 for various operating frequencies.

A comparison of the CPU run times and peak memory usages for computing the results of the SE_x^E at frequencies f = 1.5 GHz, 2 GHz, and 2.5 GHz are reported in Table. 1. A study of the data in this table shows the efficiency of the proposed method. This is due to the fact that the proposed method, only treats the interfaces of the structure with surface meshes, whereas the FE solver involves all layers and interfaces simultaneously with volume discretization technique.

TABLE 1

CPU Times And Peak Memory Usage for Computing the Results of the Electric Shielding Effectiveness (SE_x^E), Fig. 5, at Various Frequencies

Frequency (GHz)	CPU Times (s)		Peak Memory Usage (MB)	
	Proposed Method	FE Method [24]	Proposed Method	FE Method [24]
1.5	34.0	3964.6	109.2	36825.6
2	47.5	6562.0	124.5	47254.1
2.5	53.4	8579.7	153.4	60412.3

The study of the data given in Table. 1 demonstrates that the CPU execution time and memory usage tend to rise as the operating frequency increases. Notice that by increasing the operating frequency, the wavelength tends to decrease. This leads to finer meshes for accurate modeling of the

structure and representation of $\vec{J}$ and $\overrightarrow{M}$ at the interfaces. For SIE-MoM solution, this equals to a larger number of surface-meshes which, in turn, forms a larger impedance matrix. As a result, the computation time and memory usage for inversion of the impedance matrix and the solution of the problem increase. For finite-element method, the number of volume-meshes for handling all layers and interfaces increases tremendously, which subsequently increases the computational load.

3-2-Two-Layer Cubic Anisotropic Composite Enclosure

Having represented the computation efficiency for anisotropic composite enclosures, we examine a two-layer cubic composite enclosure as a common industrial object. Referring to Fig. 6, the dimensions of the cubic structure are as follows, $a = b = c = 80$ mm, $w_1 = 2.5$ mm, and $w_2 = 7.5$ mm. The structure illumined by a unit $\hat{z}$ -polarized plane wave propagating in the direction of x. The host material in the inner ($s_1 = 0.55$ mm and $d_1 = 0.25$ mm) and outer layers ($s_2 = 1.5$ mm and $d_2 = 0.4$ mm) are considered Teflon ($\varepsilon_{r,t} = 2.2$) and epoxy resin ($\varepsilon_{r,e} = 3.4$), respectively. Also, the reinforcing phase in both layers is cylindrical carbon fibers with $\varepsilon_{r,c} = 4$ and the electrical conductivity of $\sigma_{f_{1,2}} = 70000$ S/m. Accordingly, the fiber volume fraction in the inner (reflecting) layer will be $v_1 = 3.57$ %, whereas it is higher value of $v_2 = 1.11$ % in the outer (absorbing) layer. Finally, the orientation of fibers in the reflecting and absorbing layers are parallel to *x*- and *y*-axis, respectively.

The frequency dependence behaviors of equivalent perpendicular and parallel relative permittivity of both layers are shown in Fig. 7, where the perpendicular components of the reflecting layer have excessively large value of the imaginary part causes strong loss in smaller thickness ($w_1 = t_1 = 2.5$ mm).

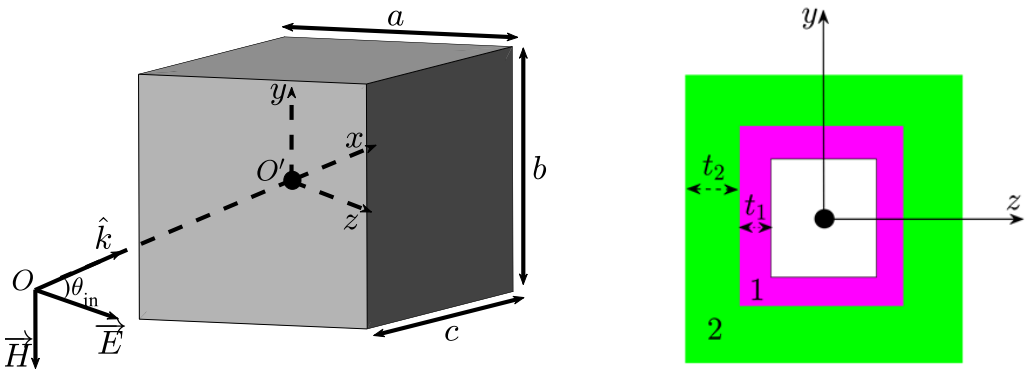

(a) (b)

Fig. 6. (a) 3D and (b) 2D views of a two-layer cubic anisotropic composite enclosure.

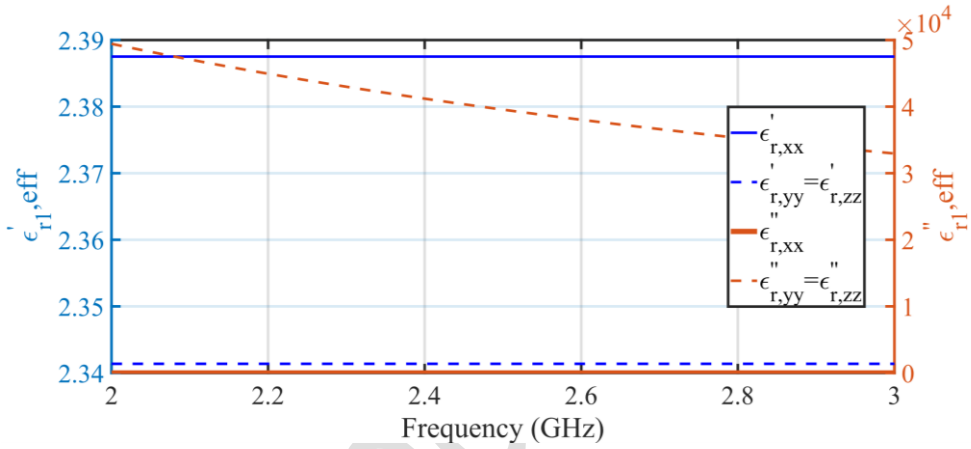

(a)

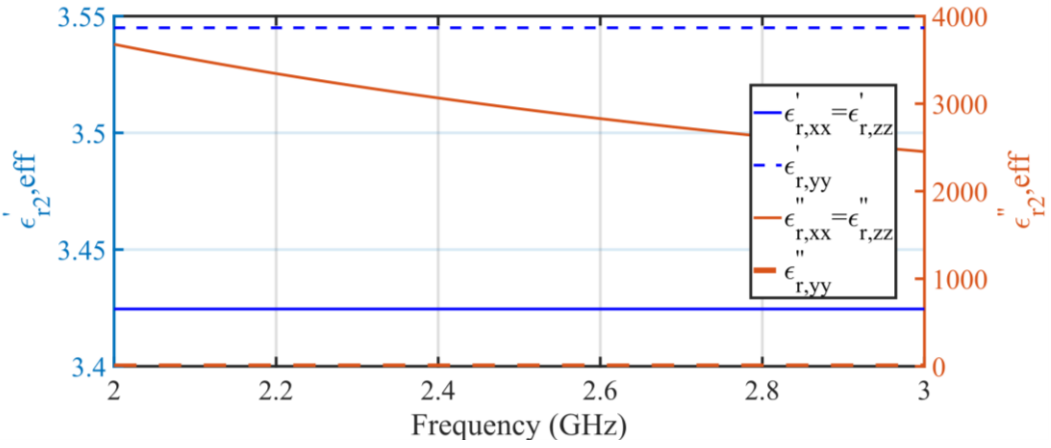

(b)

Fig. 7. Frequency dependence of real ($\varepsilon'_{r,eff}$) and imaginary ($\varepsilon''_{r,eff}$) parts of the equivalent perpendicular and parallel relative permittivity of a) the reflecting, and b) the absorbing anisotropic composite layers of the structure shown in Fig. 6.

10.22060/EEJ.2026.25436.5932

Variations of the *z*-component of the electric shielding effectiveness (SE_z^E) of the enclosure shown in Fig.6 are plotted in Fig. 8 and compared to those obtained using FE code of CST studio. This comparison further confirms the validity of the implemented method. The reason for obtaining a good SE for the *z*-component of electric field depends on the orientation of reinforcing fibers in both layers. The electric tangent loss in the both layers is very large (up to 10^4) for directions perpendicular to the axis of the reinforcing fibers, *i.e.*, *y*- and *z*-directions in reflecting layer and *x*- and *z*-directions in absorbing layer. As a result, both layers exhibit very large value of loss against the polarization of the incident wave ($\vec{E}_z$) and SE_z^E improves significantly.

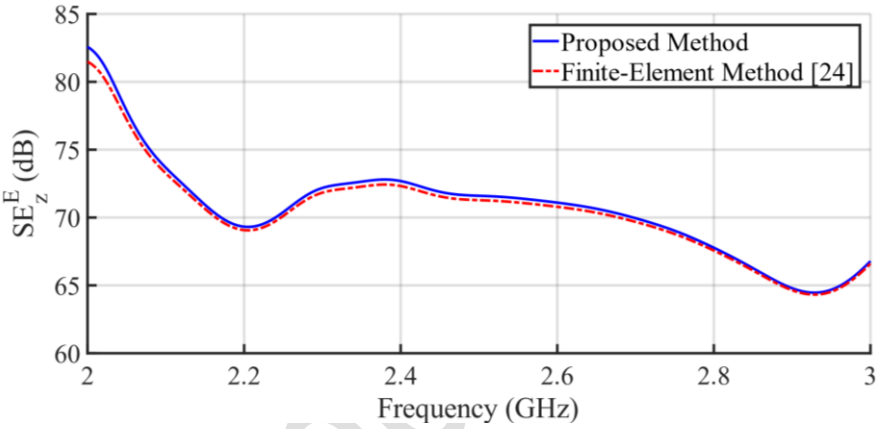

Fig. 8. Variations of the *z*-component of the electric shielding effectiveness (SE_z^E) at the center of the cubic enclosure shown in Fig. 6 for various operating frequencies.

To study the effects of the diameter of the cylindrical reinforcing fibers, the thickness of various layers, the relative permittivity of the matrix phase of layers, the electrical conductivity of the fibers, and the polarization of the incident plane wave on SE of the cubic enclosure, a set of sensitivity analysis is performed. At first, we vary the diameter of the reinforcing carbon fibers of the reflecting (d_1) and then, absorbing (d_2) layers from 0.15 mm to 0.5 mm, and 0.4 mm to 0.8 mm, respectively, while keeping other parameters unchanged at every analysis. The variations of the electric SE, SE_z^E, for both layers are plotted in Figs. (9a) and (9b).

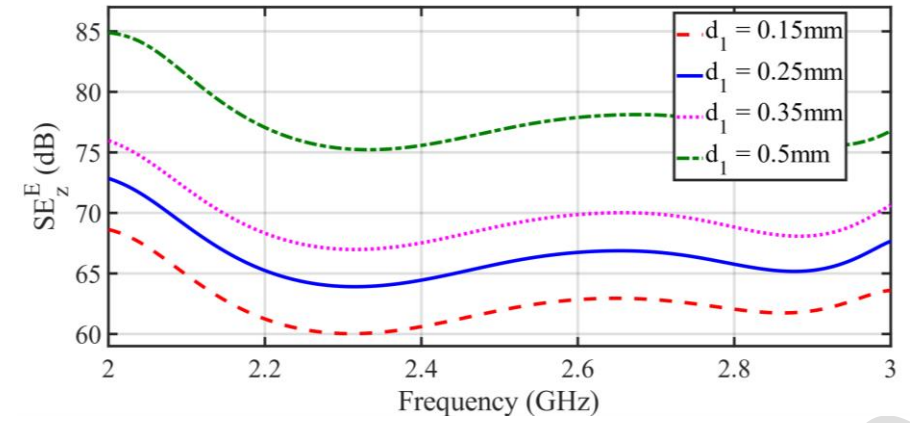

(a)

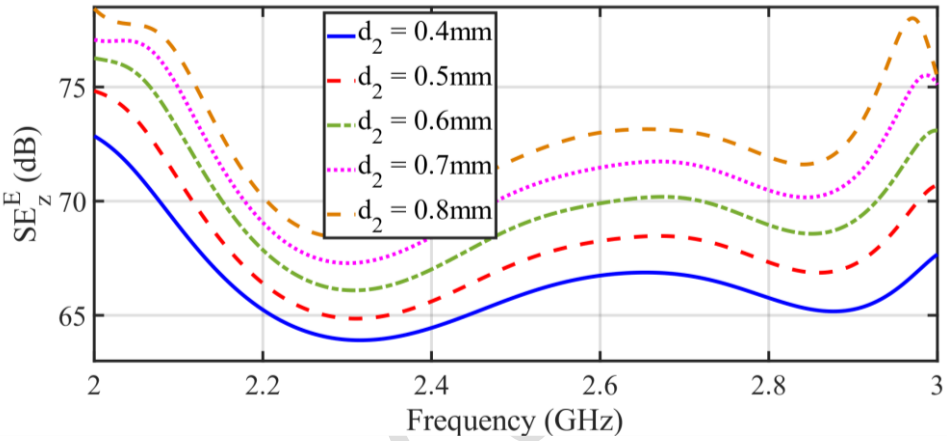

(b)

Fig. 9. Effect of the diameter of the reinforcing carbon fibers of the a) reflecting layer (d_1), and b) absorbing layer (d_2) on the electric shielding effectiveness (SE_z^E) of the cubic enclosure shown in Fig. 6.

It can be deduced from the results of Fig. 9 that increasing both d_1 and d_2 will increase the SE; but the diameter of fibers in reflecting layer is more effective than absorbing layer in the improvement of SE. The main reason for this improvement is increasing the fiber volume fraction from v_1= 1.28 % to high value of v_1= 14.3 % for reflecting layer and from v_2= 1.11 % to v_2= 4.47 % for absorbing one. Increasing the volume fraction of lossy conductive fibers will increase the imaginary part of the equivalent perpendicular permittivity of the layers which, in turn, increases the electric tangent loss and reduces wave penetration. No significant frequency shift for the results of Fig. (9a) is because of the very small resultant real part of the equivalent perpendicular relative permittivity of the dominant reflecting layer compared to the excessively large of imaginary part values. Conversely, the real part of the equivalent perpendicular relative permittivity of the absorbing layer against to the smaller

10.22060/EEJ.2026.25436.5932

values of imaginary part shows its effect as a movement of the diagrams in the Fig. (9b) due to the effective electrical length phenomena.

Next, we vary the thickness of reflecting layer (w_1) from 1 mm (v_1= 8.92 %) to 3 mm (v_1= 2.97 %) and then, absorbing one (w_2) from 6.5 mm (v_2= 1.28 %) to 8.5 mm (v_2= 0.98 %), while maintaining other parameters unchanged. A study of the results shown in Fig. 10(a) indicates that the SE value of the enclosure has reduced by at least 5 dB by increasing of the value of w_1. Similar effects are made when w_2 is increased. As can be seen from Fig. 10(b), with 2 mm increase in the value of w_2, the SE has decreased by at least 6.26 dB. It is obvious that by increasing the layer thickness while keeping the fiber diameter (d) and the center-to-center distance of adjacent fibers (s) constant, the effect of the lossless dielectric matrix becomes dominant and according to (4c), the volume fraction of fibers or loss value decreases. This leads to reducing the SE. On the other hand, due to the greater thickness that was initially considered for the absorbing layer, its variations cause a greater prevalence of the lossless dielectric matrix phase effects compared to the reflecting layer. Another noteworthy point is the frequency shift of the SE in Fig. 10(b), which is due to the dominance of the matrix phase effect and the change in phase velocity.

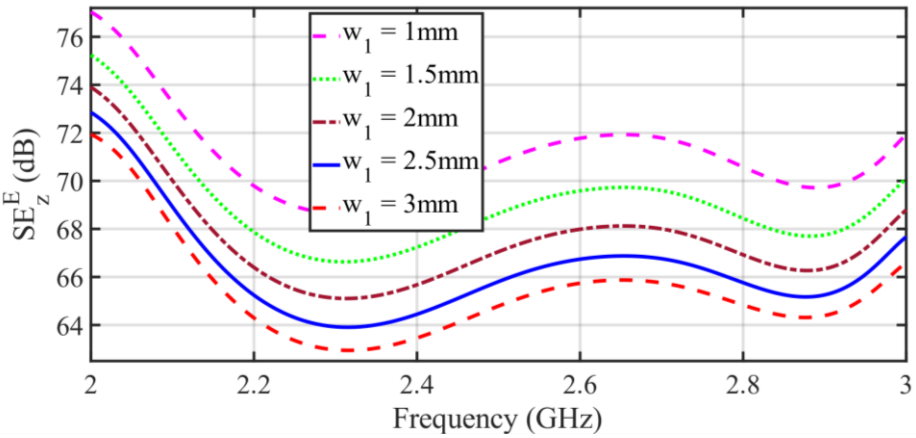

(a)

10.22060/EEJ.2026.25436.5932

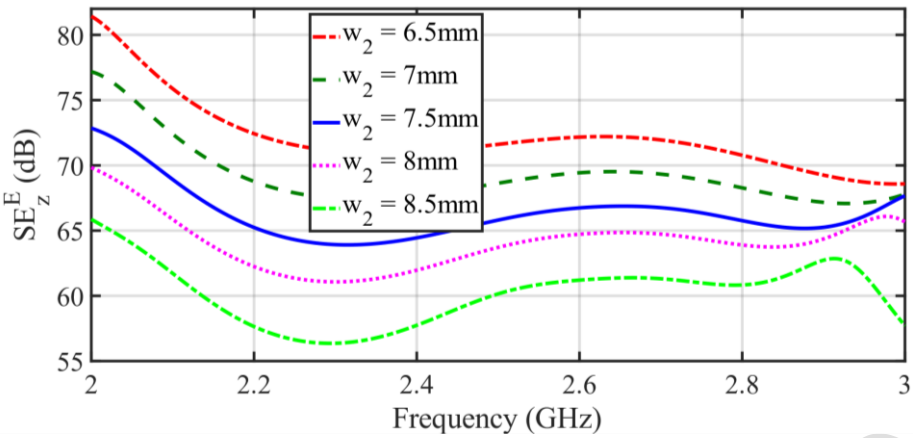

(b)

Fig. 10. Effect of the thickness of the a) reflecting layer (w_1), and b) absorbing layer (w_2) on the electric shielding effectiveness (SE_z^E) of the cubic enclosure specified in Fig. 6.

Now, we increase the matrix relative permittivity of the reflecting layer ($\varepsilon'_{r,m1}$) from 1.5 to 12. The variations of the electric SE, SE_z^E, are presented in Fig. 11(a). It should be noted that since the geometric parameters have not changed, the volume fraction of the fibers (v_1) will remain the same in all results (see (4c)). On the other hand, due to the very small values of $\varepsilon'_{r,m1}$ compared to the very high value of loss where an example of which is shown in Fig. 7, we will not have a frequency shift in the SE results. Also, with the large increase in the value of $\varepsilon'_{r,m1}$, the maximum reduction in SE will be about 2.22 dB. Therefore, it can be said that the changes in the $\varepsilon'_{r,m1}$ will not have a significant effect on SE. Similar study is done by increasing the relative permittivity of the matrix phase of absorbing layer ($\varepsilon'_{r,m2}$) from 1.5 to 12. The SE variations are plotted in Fig. 11(b). Here, unlike the reflecting layer, which has very large loss in the order of 10^4 and the dielectric constant of the matrix phase has small effect on the SE, the dielectric constant of the matrix, along with the larger thickness of the layer, have a greater effect on the loss value and consequently SE, causing drop to a maximum of 56.85 dB. Also, the increase in the value of $\varepsilon'_{r,m2}$, along with the larger thickness of the layer (w_2= 7.5 mm), lead to a greater frequency shift in the obtained results.

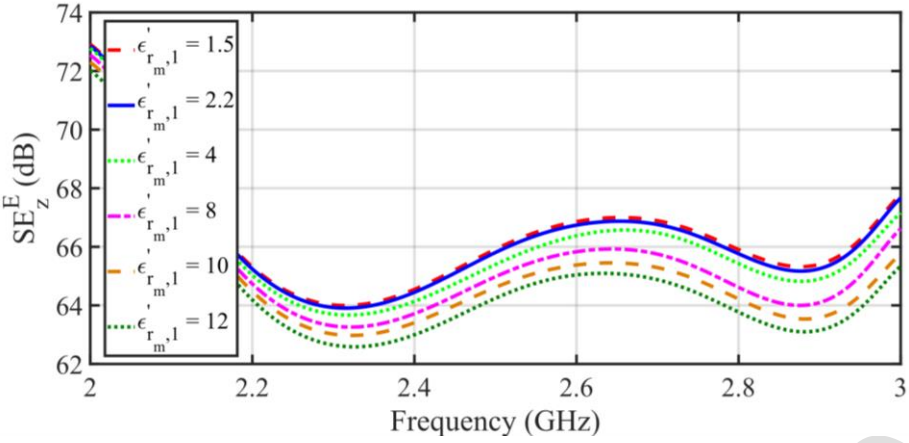

(a)

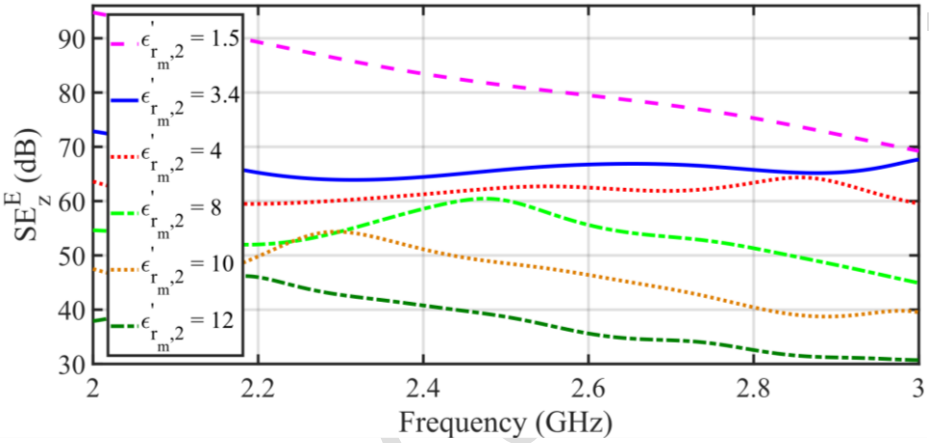

(b)

Fig. 11. Effect of the matrix phase relative permittivity of the a) reflecting layer ($\varepsilon'_{r,m1}$), and b) absorbing layer ($\varepsilon'_{r,m2}$) on the electric shielding effectiveness (SE_z^E) of the cubic enclosure specified in Fig. 6.

Next, we increase the electrical conductivity of reinforcing fibers embedded in the reflecting layer ($\sigma_{f,1}$) from 17500 S/m to 280000 S/m, and for absorbing layer ($\sigma_{f,2}$) from 1250 S/m to 40000 S/m, separately. The variations of SE are shown in Fig. 12.

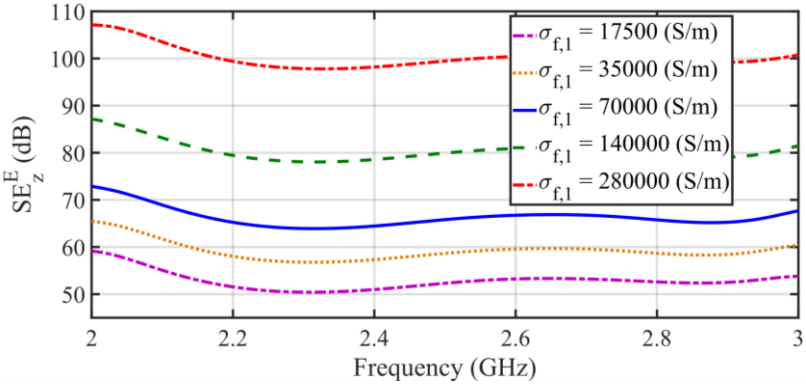

10.22060/EEJ.2026.25436.5932

(a)

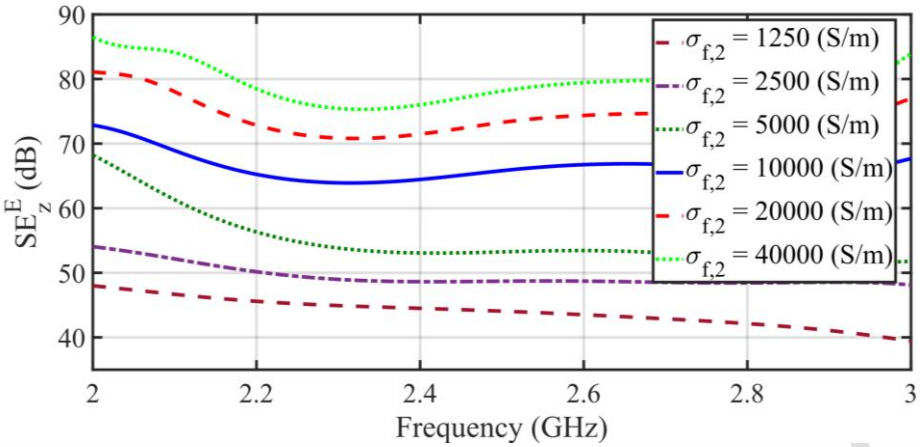

(b)

Fig. 12. Effect of the electrical conductivity of reinforcing fibers of the a) reflecting layer ($\sigma_{f,1}$), and b) absorbing layer ($\sigma_{f,2}$) on the electric shielding effectiveness (SE_z^E) of the cubic enclosure specified in Fig. 6.

From the results of Fig. 12(a), we deduce that with the increase in the value of $\sigma_{f,1}$ up to 16-times at a lower thickness of the reflecting layer, the SE increases to a maximum value of 107.5 dB at a frequency of 2 GHz, which is about 48.5 dB more than the SE value for the electrical conductivity of 17500 S/m at the same frequency. Clearly, this extraordinary improvement is due to the increase in the reflecting layer loss due to the increase in the electrical conductivity which decreases the wave penetration into the enclosure.

Also, according to Fig. 12(b), with an increase in the value of $\sigma_{f,2}$ up to 32-times in the greater thickness of the absorbing layer, the maximum increase in the SE value is 44.5 dB at a frequency of 3 GHz, which is similar to the increasing effect of SE with increasing the value of $\sigma_{f,1}$. In general, it can be concluded that for proper shielding design, a compromise between the thickness of the layer and the electrical conductivity of the reinforcing fibers is necessary. Therefore, from the above observations, it is clear that a layer with a thinner thickness and a higher density of fibers requires less increase in the electrical conductivity of the fibers (16-times) to achieve a high SE; but conversely, a thicker layer with a lower density of fibers requires more incremental changes in the conductivity of the fibers (32-times) to receive a suitable SE. On the other hand, due to the lower conductivity and

then, electrical loss in absorbing layer compared to the reflecting layer, the real part of the equivalent permittivity will show its effect in the form of a frequency shift in the results.

One of the points that should be considered in the construction of multilayer composite shielding enclosures is their ability against to the plane wave incidence with unknown polarization. Therefore, in this section, we will examine the effect of the polarization of the incident wave on the SE of the enclosure. According to Fig. 7, for a two-layer composite structure shown in Fig. 6, the loss values of the enclosure walls along the *z*-axis are stronger than the others ($tan\delta_{zz} \gg tan\delta_{yy} \gg tan\delta_{xx}$). In addition, since the polarization of the incident plane wave was vertical ($\vec{E}_z$), the *z*-component of the electric field inside the enclosure become very small and SE_z^E found good values.

Now, Referring to Fig. 6, we move the vertical electric field by deviation angle of α^0, *i.e.*, $\vec{E}_z$ at $\alpha = 0^0$ to $\vec{E}_y$ at $\alpha = 90^0$, on the *y*-*z* plane (fixed transverse plane). This will make the incident electric field consists of both *z*- and *y*-components. The variations of the vertical electric shielding effectiveness, SE_z^E, for different angles of deviation, α^0, are plotted in Fig. 13. As found from the results of this figure, by increasing the angle of α and moving away from the *z*-axis which is perpendicular to the fibers of both reflecting and absorbing layers, only the *z*-component of electric field in the center of the enclosure increases (other components are zero) and consequently, SE_z^E, reduces. In fact, it can be said that increasing the angular distance from the axis perpendicular to the fibers of both layers ($\hat{c} = \hat{z}$), and approaching to the parallel axis of fibers in the outer absorbing layer ($\hat{c} = y$) which has the largest value of loss after the perpendicular *z*-axis of reflecting layer, the SE reduces due to the smaller value of loss of both layers. On the contrary, the closer incident electric field to the direction perpendicular to the fiber axis of both layers (smaller α) causes the greater SE. In general, due to the different directions in which the reinforcing fibers of both layers are located, we see different values of loss from the fibers in different directions, and the polarization of the electric field in the center of the cubic enclosure will no longer be the same as the polarization of the incident wave.

10.22060/EEJ.2026.25436.5932

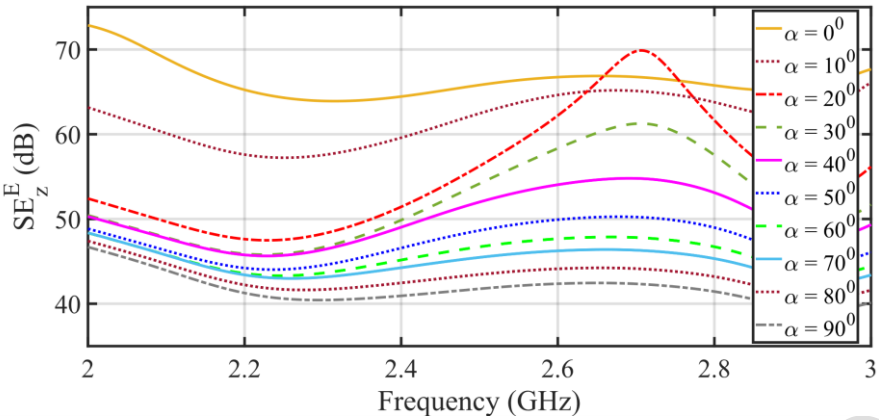

Fig. 13. Effect of the incident plane wave polarization, including *y*- and *z*-components with increasing the angular distance (α^0) by moving from *z*- to *y*-axis, on the electric shielding effectiveness (SE_z^E) at the center of the cubic enclosure specified in Fig. 6.

Next, we rotate the transverse plane of incidence (*y*-*z* plane) to create the oblique incidence through varying the angle of incidence θ by moving the direction of the incident electric field from near the *x*-axis (θ = -5^0) to near the *z*-axis (θ = -85^0) in the assigned global coordinates shown in Fig. 1, using the rotation of the boundary conditions, and the dyadic Green's functions in (7). The variations of SE along the *x*- and *z*-axis are shown in Figs. 14(a) and 14(b), respectively. What can be seen from the plots of Fig. 14 is that at θ = -5^0, since the *x*-component of the incident electric field is more dominant than *z*-component and on the other hand, since the effective loss of both layers is more dominant in the *z*-direction, the *z*-component of the internal field becomes much less than *x*-component, SE_z^E takes on a very large value (between 95 dB and 115 dB) and SE_x^E becomes small. This is also true for θ = -25^0. For θ = -45^0, the *x*- and *z*-components of the incident electric field are equal; but due to the very large loss that exist in the *z*-axis compared to the *x*-direction, SE_z^E has a higher value than SE_x^E. Then, as we move away from the *x*- and arrive closer to the *z*-axis (θ = -65^0 and -85^0), the *x*-component of the incident electric field is weaker than the *z*-component, SE_x^E increases to a maximum of about 60 dB. This is while, as the *z*-component becomes stronger up to 0.99 V/m at θ = -85^0, SE_z^E decreases compared to other angles; but due to the large loss in the *z*-direction, it will be higher than SE_x^E.

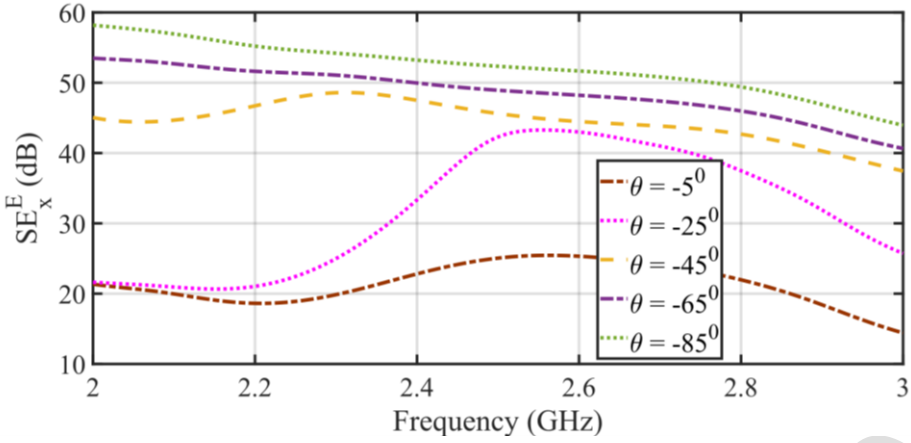

(a)

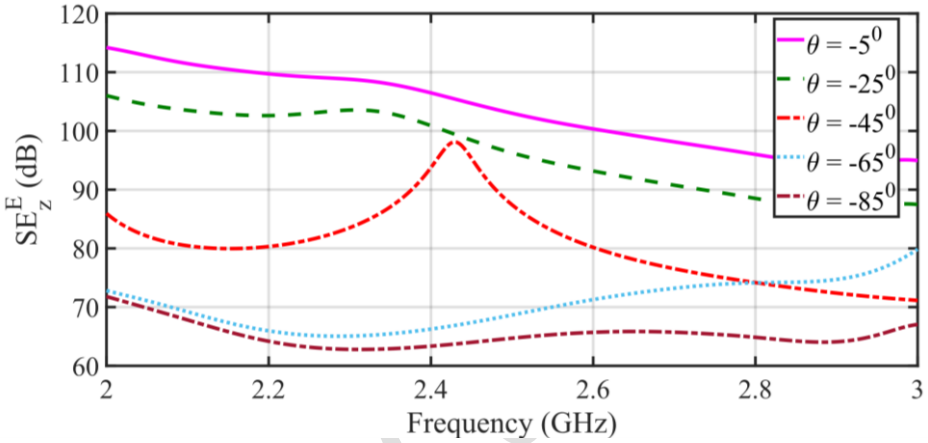

(b)

Fig. 14. Effect of the oblique incidence plane wave with change in the vertical angle of θ on the a) *x*-component, and b) *z*-component of electric shielding effectiveness at the center of the cubic enclosure specified in Fig. 6.

4. Conclusion

In this paper, we use of an efficient SIE-MoM method to study the electromagnetic shielding effectiveness of multilayered arbitrary-shape anisotropic composite enclosures. The method models each anisotropic composite layer as an equivalent homogeneous anisotropic media with tensorial characteristics. Also, it individually treats each layer via using the surface equivalence theorem. By applying the proper boundary conditions, the SIEs converted to the respective matrix equations solved by the Galerkin's-MoM. The main feature of this process is using the rotated dyadic Green's functions of the infinite space filled with the equivalent anisotropic material of the layer of interest, where the rotation angle is the angular deviation between the specified global coordinate system and

the local principal system of anisotropic layer which determined by diagonalizing the equivalent permittivity tensor in the global coordinate system. Finally, to find the unknown surface current densities, the sparse block-tridiagonal impedance matrix is inverted using an efficient block-block inversion process, which increases the speed of problem solution, significantly. The validity and efficiency of the presented method for composite structures are demonstrated for a three-layer irregular-shape anisotropic composite structure, through comparing the obtained results with those obtained by FE-solver of CST studio. Finally, a set of sensitivity analysis is done to examine the various parameters which affect the shielding properties of a two-layer cubic anisotropic composite enclosure.

It should be noted that the method can also be used for investigating the electromagnetic properties of a multilayered, arbitrarily shaped anisotropic magnetic object. This will be a future research idea.

References

[1] D. Tabor, *The Hardness of Metals*, Oxford, U.K.: Clarendon, 1951.

[2] B. N. Popov, *Corrosion Engineering: Principles and Solved Problems*, New York, NY, USA: Elsevier Press, 2015.

[3] D. Gay and S. V. Hoa, *Composite Materials: Design and Applications*, 2nd ed. Boca Raton, FL: CRC Press, 2007.

[4] H. W. Ott, *Electromagnetic Compatibility Engineering*, Hoboken, NJ, USA: Wiley Press, 2009.

[5] P. B. Jana, A. K. Mallick, S. K. De, and M. Used, "Effects of sample thickness and fiber aspect ratio on EMI shielding effectiveness of carbon fiber filled polychloroprene composites in the X-band frequency range," *IEEE Trans. Electromagn. Compat.*, vol. 34, no. 4, pp. 478-481, Nov. 1992.

[6] X. Luo and D. D. L. Chung, "Electromagnetic interference shielding using continuous carbon-fiber carbon-matrix and polymer-matrix composites," *Compos. B, Eng.*, vol. 30, no. 3, pp. 227-231, Apr. 1999.

[7] M. Kalantari and S. H. H. Sadeghi, "An efficient method for computing the shielding effectiveness of arbitrary-shape multilayered composite enclosures," *IEEE Trans. Electromagn. Compat.*, vol. 66, no. 2, pp. 444-452, Apr. 2024.

[8] D. J. Kozakoff, *Analysis of Radome-Enclosed Antennas*. Norwood, MA, USA: Artech House, 1997.

[9] C. R. Paul, *Introduction to Electromagnetic Compatibility*, New York, NY, USA: Wiley Press, 2006.

[10] M. Y. Koledintseva, J. Drewniak, and R. DuBroff, "Modeling of shielding composite materials and structures for microwave frequencies," *Prog. Electromagn. Res. B.*, vol. 15, pp. 197-215, Jun. 2009.

[11] A. H. Shivola, *Electromagnetic Mixing Formulas and Applications*, London, U.K.: IEE Press, 1999.

[12] C. L. Holloway, M. S. Sarto, and M. Johansson, "Analyzing carbon-fiber composite materials with equivalent-layer models," *IEEE Trans. Electromagn. Compat.*, vol. 47, no. 4, pp. 833-844, Nov. 2005.

[13] M.-S. Lin and C. H. Chen, "Plane-wave shielding characteristics of anisotropic laminated composites," *IEEE Trans. Electromagn. Compat.*, vol. 35, no. 1, pp. 21-27, Feb. 1993.

[14] M. R. Forouzeshfard, M. Mohebbi, and A. Mollaei, "Scattering cross section in a cylindrical anisotropic layered metamaterial," *Opt. Commun.*, vol. 407, pp. 193-198, Jan. 2018.

[15] Y.-L. Geng, X.-B. Wu, L.-W. Li, and B.-R. Guan, "Electromagnetic scattering by an inhomogeneous plasma anisotropic sphere of multilayers," *IEEE Trans. Antennas Propag.*, vol. 53, no. 12, pp. 3982-3989, Dec. 2005.

[16] M. N. O. Sadiku, *Numerical Techniques in Electromagnetics*, FL, Boca Raton: CRC Press, 2001.

[17] J. Wang, B. Zhou, L. Shi, C. Gao, and B. Chen, "Analyzing the electromagnetic performances of composite materials with the FDTD method," *IEEE Trans. Antennas Propag.*, vol. 61, no. 5, pp. 2646-2654, May. 2013.

[18] G. A. Achkar, L. Pichon, L. Daniel, and N. Benjelloun, "Effective electromagnetic properties of woven fiber composites for shielding applications," *IEEE Trans. Electromagn. Compat.*, vol. 62, no. 4, pp. 1082-1089, Aug. 2020.

[19] J. L. Volakis and K. Sertel, *Integral Equation Methods for Electromagnetics*, Raleigh, NC, USA: SciTech Press, 2012.

[20] G. Kobidze and B. Shanker, "Integral equation based analysis of scattering from 3-D inhomogeneous anisotropic bodies," *IEEE Trans. Antennas Propag.*, vol. 52, no. 10, pp. 2650-2658, Oct. 2004.

[21] E. Zareian-Jahromi, S. H. H. Sadeghi, R. Sarraf-Shirazi, R. Moini, and H. Karami, "Image solution for the 3-D static Green's function of a vertically stratified two-layer half-space", *IEEE Trans. Antennas Propag.*, vol. 64, no. 10, pp. 4336-4342, Oct. 2016.

[22] W. C. Gibson, *The Method of Moments in Electromagnetics*, Boca Raton, FL, USA: CRC Press, 2015.

[23] M. Kalantari and S. H. H. Sadeghi, "An efficient method of moments for analysis of electromagnetic scattering from a multilayered arbitrary-shape anisotropic dielectric object," *IET Microw. Antennas Propag.*, vol. 18, no. 12, pp. 1069-1083, Dec. 2024.

[24] Microwave Studio, Computer Simulation Technology (CST), 2023. [Online]. Available: www.3ds.com.